

Study of Analytical Current Ripple of Three-Phase PWM Converter

Dong Jiang, Fei (Fred) Wang

The Min H. Kao Department of Electrical Engineering and Computer Science

The University of Tennessee

Knoxville, TN, 37996, USA

Abstract—The effects of the current ripple of three-phase PWM converters are very important for the design and control of this kind of converter, which is the most popular topology for the energy conversion system. Based on the previous study of single-phase converter's current ripple, analytical current ripple of three-phase converter is studied in this paper with the Thevenin equivalent circuit of 8 different voltage vectors. With the analytical expression, current ripple peak value and RMS value could be predicted and fit the simulation results and experimental results well. This analysis provides the basis for variable switching frequency PWM method discussed in the paper of “Variable Switching Frequency PWM for Three-phase Converter for Loss and EMI Improvement” in APEC 2012.

I. INTRODUCTION

Three-phase voltage-source pulse-width-modulation (PWM) converters are among the most widely used power electronics converters for power conversion application in many area[1]. In current applications, three-phase (voltage-source) converters are widely used for AC motor drives[2], PWM rectifiers [3][4], grid connected converters[5][6] and renewable energy converters[7][8]. Different kinds of PWM methods can be used for three-phase converters. Space vector PMW (SVPWM) and discontinuous PWM (DPWM) are two typical modulation methods[9]-[12].

Usually, switching frequency is fixed for PWM methods for three-phase converters. There are several reasons to use constant switching frequency PWM. First, the realization is easier in micro controller. Second, it is easier for filter design to attenuate certain harmonics. For converter thermal design issue, with constant switching frequency, switching losses are easier to control and the design could be based on the loss calculation. However, simply treating the switching frequency to be constant could lose an important freedom for system performance improvement. Also, because switching energy converges to the harmonics of switching frequency, the electromagnetic interference (EMI) noise peak values

will also be high around these frequencies, making the EMI problem serious. Beside the constant switching frequency PWM (CSFPWM), variable switching frequency PWM (VSFPWM) is going to be developed to utilize the freedom of switching frequency. This paper is the first part of the two papers discussing the current ripple arrangement based variable switching frequency PWM. This part mainly deals with the principle of ripple current distribution in three-phase PWM converters as the basis for the part II of the two papers.

Current ripple is an important requirement for design and control of three-phase PWM converters. CSFPWM generates current ripple which is not equally distributed. Compared with CSFPWM, VSFPWM could achieve better current performance with the extra variable of switching frequency.

For recent VSFPWM methods for three-phase PWM converter, a general problem is lacking theoretically analysis of current ripple. Therefore the switching frequency variation laws cannot be designed to precisely arrange the current ripple. Reference [11] and [12] discussed the harmonic flux and Harmonic Distortion Function (HDF) to evaluate the ripple current, but mainly studied the overall effect but not ripple current distribution in time-domain. Reference [17] and [18] proposed current ripple improved PWM methods by arranging the pulses position in each switching period. These papers have studied the details of current ripple in each switching period, but keeping the constant switching frequency and have not studied the current ripple distribution. Reference [19] and [20] extended these concepts to five-phase voltage-source converter and studied their influence on the Total Harmonic Distortion (THD), but do not fully study the current ripple distribution.

Based on the detailed analysis of ripple current distribution, reference [21] proposed variable switching frequency method for single-phase inverter. The ripple current in each switching cycle could be predicted with the duty cycle d , switching period T_s , output inductance L and DC voltage V_{dc} . Then the switching frequency could be arranged to control the current ripple to satisfy certain requirements including peak current ripple and RMS current

ripple requirement. With the proposed VSFPWM methods, switching losses of single phase converter could be reduced together with satisfying the ripple requirement.

The case of ripple current in three-phase converter is more complex than single phase since the ripple current in each phase is impacted by the switching actions for all three phases. This paper extends the similar principle of reference [21] to three-phase converter to further study the ripple current distribution for this kind of converters and establish the basis for VSFPWM methods for the paper “Variable Switching Frequency PWM for Three-phase Converter for Loss and EMI Improvement”. After the introduction, the current ripple analytical expressions are studied in Section II, based on eight different Thevenin equivalent circuits for the eight different voltage vectors. The ripple current peak value and RMS value are compared in Section III, and verified with simulation results. Experimental platform is built and experimental results are shown in Section IV to verify the theoretical analysis. Finally conclusions are made in Section V to be prepared for VSFPWM development.

II. CURRENT RIPPLE ANALYTICAL EXPRESSIONS

For three-phase converters, in the modulator, d_a , d_b and d_c are the duty cycles of the three phases, varying from 0 to 1. Defining the “quasi-duty cycle” d_x' which varies from -1 to 1 by $d_x' = 2d_x - 1$ ($x=a,b,c$). The output average voltage could be expressed as the product of quasi duty cycle and half DC-link voltage in (1), with reference to the DC-link mid-point.

$$\begin{cases} V_a = d_a' \frac{V_{dc}}{2} \\ V_b = d_b' \frac{V_{dc}}{2} \\ V_c = d_c' \frac{V_{dc}}{2} \end{cases} \quad (1)$$

Pick one typical switching period for example, without losing generality, assuming that $d_a > d_b > d_c$. With SVPWM, the switch state has 7 sectors, shown in Fig.1. In each of the sector, a certain combination of voltage is added in the output inductor and the current in the inductor will linearly increase or decrease in this sector, the ripple current variation in one switching cycle will also have 7 sectors, shown in Fig.2.

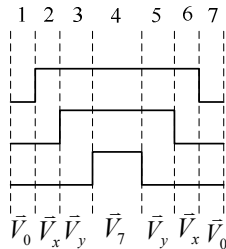


Fig.1 7 sectors in one switching cycle in SVPWM

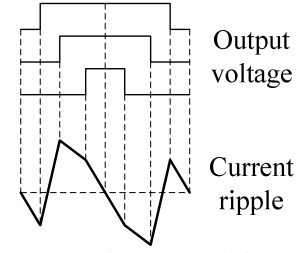


Fig.2 Ripple current variation in one switching cycle in SVPWM

For the 8 voltage vectors in three-phase converters, each voltage vector has its switches combination and equivalent circuit, shown in Fig.3. Take phase-A to be our considering phase, each of the switch equivalent circuit has its Thevenin equivalent circuit. Then the voltage drops on the inductor of phase-A could be derived for each of the voltage vector.

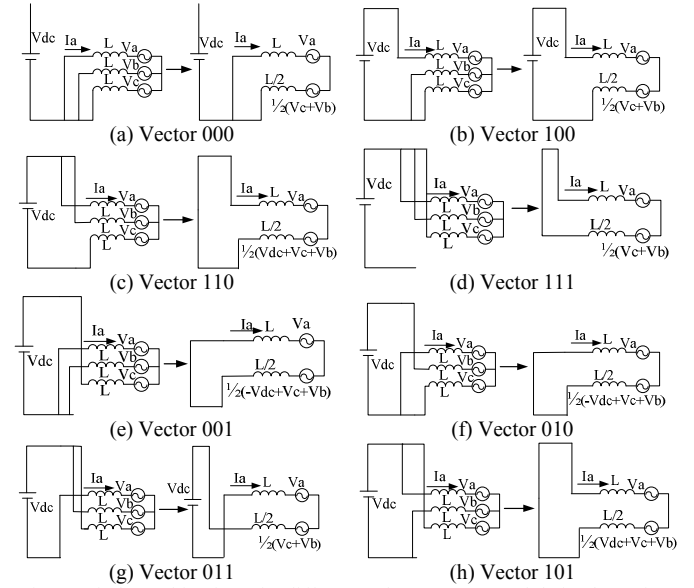


Fig.3 Switch combination of 8 different voltage vectors and their Thevenin equivalent circuits

Take the voltage vectors in Fig.1 for example. In the first sector, vector $\vec{V}_0(000)$ is added. The equivalent circuit of this switching state is shown in Fig. 3(a). Based on the Thevenin equivalent circuit of phase-B and phase-C paralleled branches, the equivalent circuit of this switching state is also shown in Fig. 3(a). Then the current slope in phase-A inductor could be derived and shown in (2), considering the average value of the phase voltage in (1), the expression could be written in (3).

$$\frac{di_a}{dt} = \frac{2}{3L} \left(\frac{V_b + V_c}{2} - V_a \right) \quad (2)$$

$$\frac{di_a}{dt} = \frac{V_{dc}}{3L} \left(\frac{d_b' + d_c'}{2} - d_a' \right) \quad (3)$$

In the second sector, vector \vec{V}_x is added, (in this case, $\vec{V}_x = (100)$), the equivalent circuit is shown in Fig. 3(b). Similar kind of Thevenin circuit is derived in Fig. 3(b), too.

The current slope is derived as (4). In the third sector, vector \vec{V}_y is added, (in this case, $\vec{V}_y=(110)$), the equivalent circuit is shown in Fig.3 (c) together with the Thevenin equivalent circuit. The current slope is derived as (5). In the fourth sector, vector $\vec{V}_7(111)$ is added, the equivalent circuit of this switching state is shown in Fig.3 (d), together with the Thevenin equivalent circuit. The slope of i_a is derived in (6).

$$\frac{di_a}{dt} = \frac{2V_{dc}}{3L} \left(1 + \frac{d_b' + d_c'}{4} - \frac{d_a'}{2}\right) \quad (4)$$

$$\frac{di_a}{dt} = \frac{2V_{dc}}{3L} \left(\frac{1}{2} + \frac{d_b' + d_c'}{4} - \frac{d_a'}{2}\right) \quad (5)$$

$$\frac{di_a}{dt} = \frac{V_{dc}}{3L} \left(\frac{d_b' + d_c'}{2} - d_a'\right) \quad (6)$$

Then in the sector 5, 6 and 7, the voltage vectors and the current slope are the same with sector 3, 2 and 1, the current ripple waveform in this switching cycle is shown in Fig. 2

In each switching-period of the three-phase converter, 4 of 8 voltage vectors are applied. Based on the Thevenin equivalent circuit in Fig.3, the slope of the current ripple could be derived and summarized in Table.1.

Table. 1 Ripple current slope with different voltage vectors

Vector	Ripple current slope
000	$\frac{di_a}{dt} = \frac{V_{dc}}{3L} \left(\frac{d_b' + d_c'}{2} - d_a'\right)$
100	$\frac{di_a}{dt} = \frac{2V_{dc}}{3L} \left(1 + \frac{d_b' + d_c'}{4} - \frac{d_a'}{2}\right)$
110	$\frac{di_a}{dt} = \frac{2V_{dc}}{3L} \left(\frac{1}{2} + \frac{d_b' + d_c'}{4} - \frac{d_a'}{2}\right)$
111	$\frac{di_a}{dt} = \frac{V_{dc}}{3L} \left(\frac{d_b' + d_c'}{2} - d_a'\right)$
001	$\frac{di_a}{dt} = \frac{V_{dc}}{3L} \left(\frac{d_b' + d_c'}{2} - 1 - d_a'\right)$
010	$\frac{di_a}{dt} = \frac{V_{dc}}{3L} \left(\frac{d_b' + d_c'}{2} - 1 - d_a'\right)$
011	$\frac{di_a}{dt} = \frac{2V_{dc}}{3L} \left(\frac{d_b' + d_c'}{4} - 1 - \frac{d_a'}{2}\right)$
101	$\frac{di_a}{dt} = \frac{2V_{dc}}{3L} \left(\frac{1}{2} + \frac{d_b' + d_c'}{4} - \frac{d_a'}{2}\right)$

Similarly, the current ripple of phase B and phase C could also be analyzed like that.

For SVPWM, as shown in Fig.4, the current ripple in one switching cycle has 7 linear parts in the whole switching cycle. The effective times for the 7 sectors are shown in Fig.4. The current ripple is anti-symmetric between first and second half. Assuming the ripple current slope for V_x and V_y are k_1 and k_2 , calculated in Table.1. The ripple current turning point values are shown in (7), the value of x and y could be either positive or negative. Then based on Fig. 4,

the peak current ripple in one switching cycle is $\max(|x|, |y|)$. The ripple current RMS value could also be derived from Fig.4, as shown in (8).

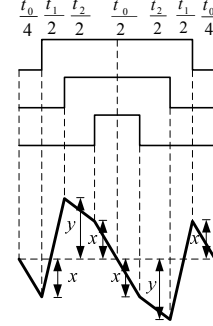


Fig.4 Current ripple in one switching cycle: SVPWM

$$\begin{cases} x = k_1 \cdot \frac{t_0}{4} \\ y = k_1 \cdot \frac{t_0}{4} + k_2 \cdot \frac{t_1}{2} \end{cases} \quad (7)$$

$$\Delta I_{rms} = \sqrt{\frac{t_0}{T_s} \frac{x^2}{3} + \frac{t_1}{T_s} \frac{x^2 + xy + y^2}{3} + \frac{t_2}{T_s} \frac{x^2 - xy + y^2}{3}} \quad (8)$$

If DPWM is used instead of SVPWM, the current ripple could be different. The ripple in one switching cycle could have 5 linear sectors. The case with DPWM will also be studied in this paper. The analytical expressions of DPWM are also studied based on the current slope in Table.1.

With DPWM, the minimum duty cycle is clamped to 0 or maximum duty cycle is clamped to 1, the corresponding current ripple in one switching cycle is shown in Fig. 5(a) and Fig.5(b). Different from SVPWM, the ripple current of DPWM only has five linear parts in one switching period.

For the DPWM in Fig.5, assuming ripple current's slope under zero vector is k_1 , the ripple current's slope under the voltage vector near the zero vector is k_2 , then the ripple current turning value could be written in (9). The current ripple peak in one switching cycle in DPWM is also $\max(|x|, |y|)$, the ripple current RMS value could also be derived from Fig.5 as (10).

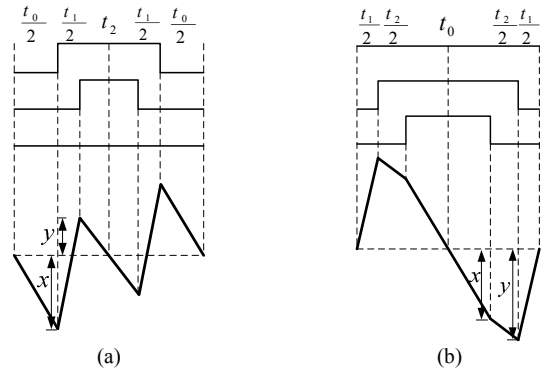


Fig.5 Current ripple in one switching cycle: DPWM (a) Clamped to negative bus, (b) Clamped to positive bus

$$\begin{cases} x = k_1 \cdot \frac{t_0}{2} \\ y = \begin{cases} k_1 \cdot \frac{t_0}{2} + k_2 \cdot \frac{t_1}{2} & (\text{Fig.5(a)}) \\ k_1 \cdot \frac{t_0}{2} + k_2 \cdot \frac{t_2}{2} & (\text{Fig.5(b)}) \end{cases} \end{cases} \quad (9)$$

$$\Delta I_{rms} = \begin{cases} \sqrt{\frac{t_0}{T_s} \frac{x^2}{3} + \frac{t_1}{T_s} \frac{y^2}{3} + \frac{t_2}{T_s} \frac{x^2 + xy + y^2}{3}} & (\text{Fig.5a}) \\ \sqrt{\frac{t_0}{T_s} \frac{x^2}{3} + \frac{t_2}{T_s} \frac{y^2}{3} + \frac{t_1}{T_s} \frac{x^2 + xy + y^2}{3}} & (\text{Fig.5b}) \end{cases} \quad (10)$$

III. RIPPLE CURRENT COMPARISON

Based on the analytical expressions developed in part II, ripple current could be predicted with the modulation method, DC-link voltage V_{dc} , output inductance L and switching frequency f_s . The ripple current unit value is $V_{dc} / (3Lf_s)$.

Fig.6 displays the analytical predicted waveform of current ripple in phase-A with SVPWM, with modulation index of 0.9 and 0.5, including the waveform in the whole line-period and the enlarged details in one switching cycle. Current ripple distribution in one line period is varying and the ripple current in one switching period follows the 7 sector principle.

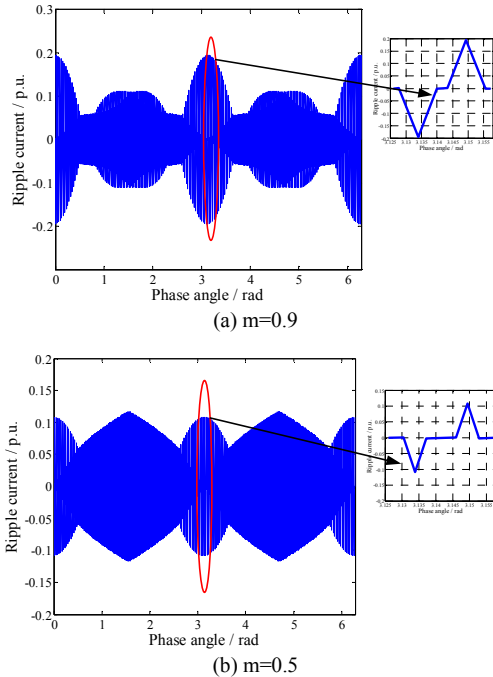


Fig. 6 Ripple current in one line-cycle: SVPWM

Similarly, ripple current could be re-constructed for DPWM, with the same cases. The theoretical predicted current ripple waveforms are shown in Fig.7, with one line-period waveform and enlarged detail in one switching cycle.

Comparing with Fig.6, the current ripple value is obviously larger with DPWM than SVPWM. The current ripple distribution is not equal either. In Fig.6, seven sectors could be found in the enlarged one switching cycle, but for DPWM, five sectors appear in the same time period in Fig.7.

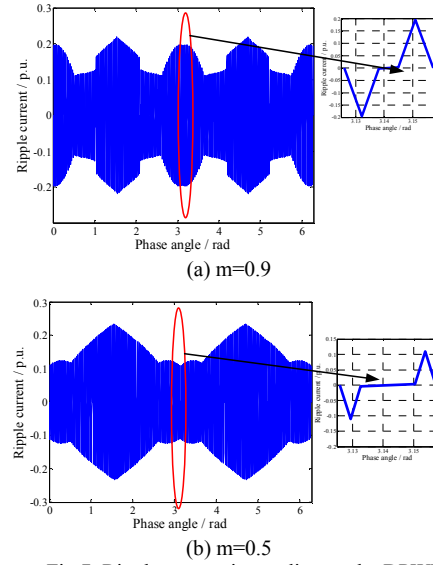


Fig.7 Ripple current in one line-cycle: DPWM

Then by sweeping the modulation index from 0.1 to 1.1, the ripple current peak-to-peak value could be predicted in Fig. 8. The ripple peak value of DPWM covers all that of SVPWM in the whole range. Fig.9 shows the comparison of ripple current RMS value (calculated by (8) and (10)) with SVPWM and DPWM with different modulation index. DPWM could generate obviously bigger ripple current RMS value than SVPWM and have bigger THD.

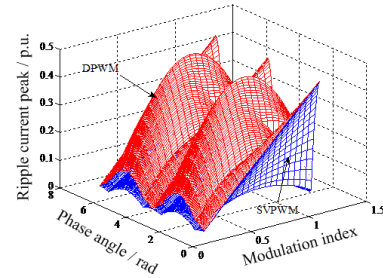


Fig.8 Comparison of ripple current peak-to-peak value

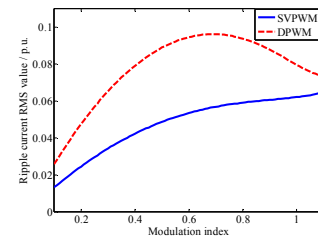


Fig.9 Comparison of ripple current RMS value

Comparison between analytical results and simulation results are studied to verify the prediction. The simulation model is simulated in MATLAB/SIMULINK as a grid-connected inverter with 400V DC-link voltage and 500 μ H out-put inductor. The system circuit is shown in Fig.10. This topology could represent general three-phase converter with AC loads like motor, grid and passive loads. Ripple current in the simulation result is defined as the error between phase-current and average model result. The predicted current ripple fits the simulation result well for both SVPWM and DPWM.

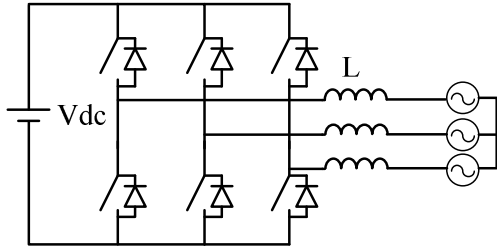


Fig. 10 Equivalent circuit for simulation

Fig.11 shows the three-phase current of the simulation results of the converter. The three phases are well balanced, without losing of generality, phase-A is selected for analysis. Fig.12 shows the phase current and its average value in one line-period (60Hz).

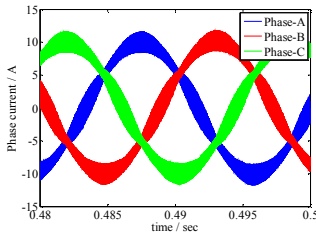


Fig.11 Simulation result: three-phase current with SVPWM (20kHz)

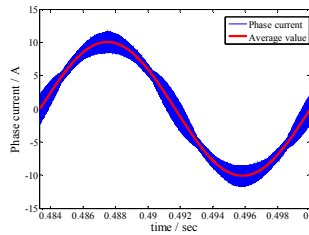


Fig.12 Simulation result: Phase current and its average value with SVPWM (20kHz)

The ripple current is the error between phase current and its average value. Fig.13 shows the ripple current in simulation and theoretical prediction in one line-period (60Hz). The enlarged details of the ripple currents are also shown in Fig.13. The overall waveform of the simulation result is very close to the theoretical predicted result, so does the enlarged details. Fig.14 shows that the theoretical predicted current ripple peak value well fits the simulation results. The ripple current RMS value is 0.798A and THD is 11.2%, well fitting the theoretical predicted value (0.803A and 11.3%).

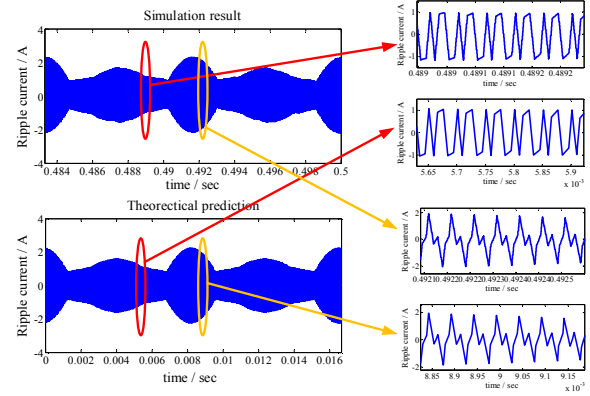


Fig.13. Comparison between simulation results and theoretical prediction with SVPWM: whole period and details

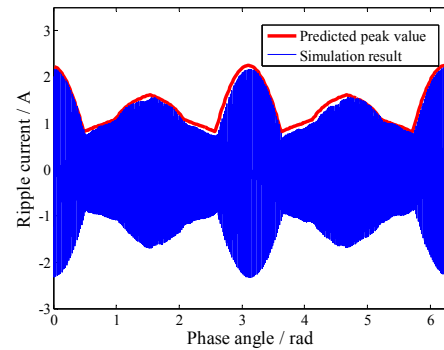


Fig.14 Comparison between theoretical predicted peak ripple and simulation results: SVPWM

Fig.15 shows the simulation results of the three-phase current with DPWM for the same case. Picking phase-A for example, the phase current and its average value is shown in Fig.16. The ripple current comparison is shown in Fig.17 with one line-period waveform and enlarged details, simulation results well fit the theoretical predicted current ripple value. The predicted ripple current peak value also fits the simulation results well in Fig.18. The simulated ripple current RMS value is 1.320A and the THD of 18.51%, which is nearly the same of the predicted results of 1.320A and 18.51%.

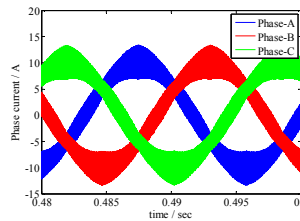


Fig.15 Simulation result: three-phase current with DPWM (20kHz)

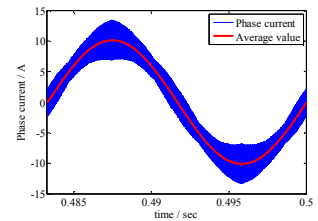


Fig.16 Simulation result: Phase current and its average value with DPWM (20kHz)

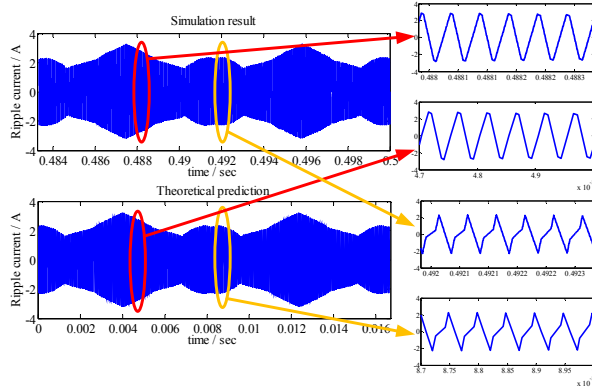


Fig.17 Comparison between simulation results and theoretical prediction with DPWM: whole period and details

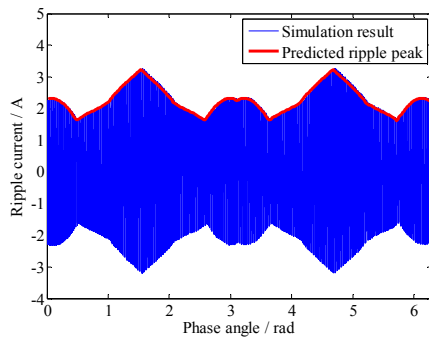


Fig.18 Comparison between theoretical predicted peak ripple and simulation results: DPWM

IV. EXPERIMENTS

In order to further verify how does the theoretical ripple current prediction compare with real ripple current in three-phase PWM converters, experimental testbed is build up. The testbed is a three-phase inverter driving L-RC load, shown in Fig.19: $L=800\mu\text{H}$, $C=27\mu\text{F}$ and $R=10\Omega$, with 6.25 kHz switching frequency. The controller is using floating point DSP of TMS320F28335 produced by TI. The switching period is updated in the interruption program. The waveforms are measured and recorded in Tektronics DPO5204 oscilloscope with 15MHz current probe TCP303. The photo of the experimental set-up is shown in Fig.20. The experiments are done with 240V DC voltage and modulation index of 0.8. Deadtime is set to be 400 μs to reduce the influence.

With R-C parallel load, the voltage drop could be treated as mainly fundamental frequency based voltage, similar with motor back-EMF or grid voltage. If only with R load, the load voltage would also have obvious ripple component and impair the linear model of the inductor current.

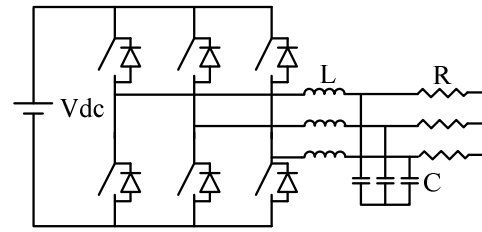


Fig.19. Experimental circuit

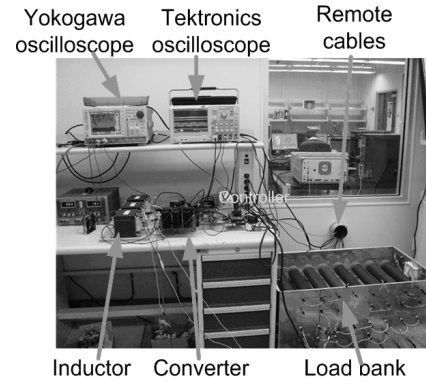


Fig.20. Picture of the testbed hardware

Experimental results of three phase current with SVPWM and DPWM are shown in Fig.21 and Fig.22. Picking phase-A to study for both SVPWM and DPWM, experimental results are selected with one line cycle. With FFT analysis, the amplitude and phase-angle of the current could be derived, and the fundamental current (average current) could be re-constructed. The comparisons of phase current and its average value are shown in Fig.23 and Fig.24.

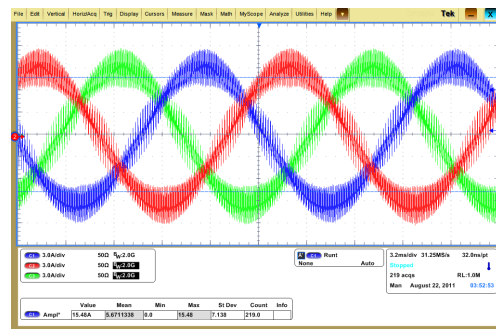


Fig.21 Experimental result: three-phase current with SVPWM

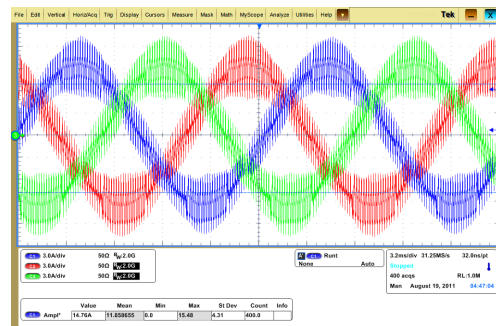


Fig.22 Experimental result: three-phase current with DPWM

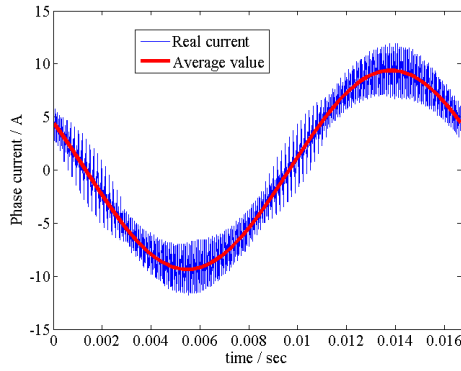


Fig.23 Experimental results: phase current and its average value with SVPWM

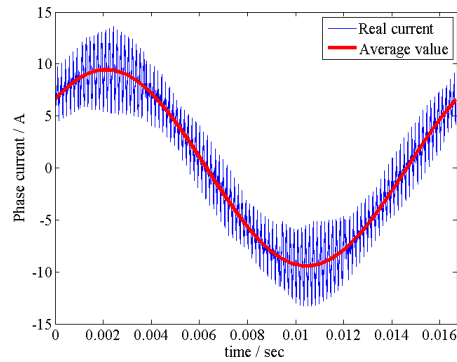


Fig.24 Experimental results: phase current and its average value with DPWM

In order to verify the proposed 7 sector and 5 sector principle of current ripple, the output inductor voltage and corresponding phase current are shown in Fig.25 and Fig.26. The details of 0.4ms (2.5 switching cycles) are shown in the right side of the two figures. With each of the voltage vector, the inductor voltage will be nearly constant and the phase current will be linearly varying. In the enlarged details, the sectors are very obvious. For SVPWM, 7 sectors are in one switching cycle, for DPWM, 5 sectors are in one switching cycle. Experimental results verify the sectors predicted ripple current variation principle.

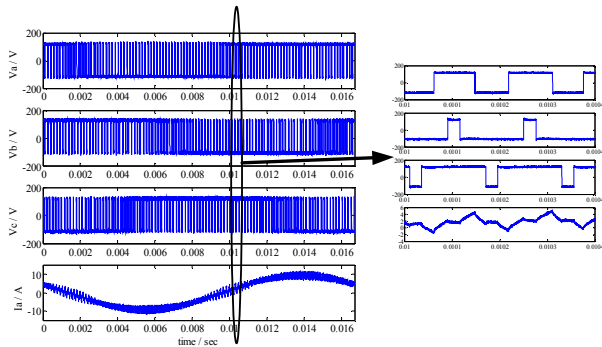


Fig.25 Experimental results: three-phase output voltage and phase-A current with SVPWM

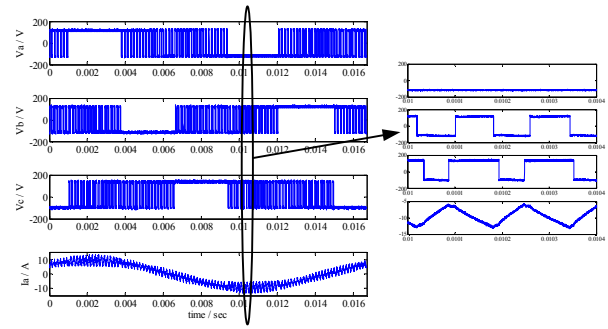


Fig.26 Experimental results: three-phase output voltage and phase-A current with DPWM

The error between phase current and its average value is the current ripple. The comparison between the current ripple of experimental results and analytical predicted ripple peak are shown in Fig.27 and Fig.28 for SVPWM and DPWM. The experimental ripple is fitting well with the predicted ripple peak value (red line).

The predicted RMS current for the SVPWM is 1.04A and the experimental result of ripple current RMS value is 1.02A; the predicted RMS current for DPWM is 1.58A and the experimental result of ripple current RMS value is 1.50A. The prediction errors are 2% for SVPWM and 5% for DPWM. The prediction errors are mainly caused by deadtime effect, parameter non-ideality and probe errors.

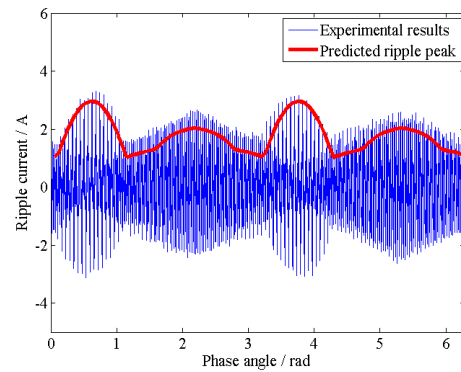


Fig.27 Experimental results of current ripple with SVPWM

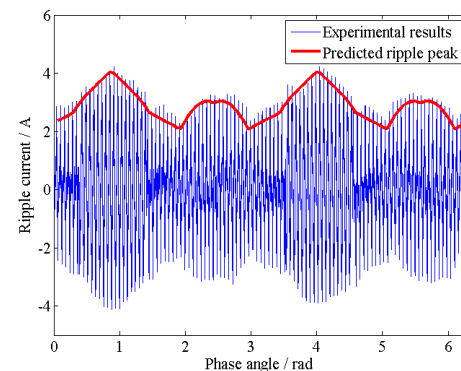


Fig.28 Experimental results of current ripple with DPWM

V. CONCLUSIONS

As the basis for variable switching frequency PWM (VSFPWM) methods, this paper aims at developing the analytical ripple current expressions for three-phase PWM converters. Following conclusions could be made:

1. With each of the voltage vector, the output current slope is constant. Based on the 8 voltage vectors in the converter, 8 Thevenin equivalent circuits are modeled to derive the current ripple with each vector. The current ripple slope is summarized in Table.1.
2. With SVPWM and DPWM, there are 7 and 5 sectors of current ripple in each of the switching cycle, which is determined by the duty cycles of each phase. Then the current ripple and its peak value and RMS value could be predicted for the whole line period. Simulation and experimental results show that the prediction is precise.
3. DPWM has obviously bigger ripple peak value and RMS value than SVPWM for the same condition, although the switching losses are effectively reduced.
4. Ripple current distribution for three-phase PWM converter is varying in one line cycle, which provides a space for further improve by switching frequency variation.

With the analytical current ripple developed in this paper, the ripple current in three-phase PWM converter could be predicted in the controller before pulses are generated, and the switching period could be adaptive for certain ripple requirement. The application of analytical ripple current method in this paper could most benefit the variable switching frequency control for three-phase PWM converter, which is discussed in the other paper in APEC 2012: Variable Switching Frequency PWM for Three-phase Converter for Loss and EMI Improvement.

Reference

- [1] T. G. Habetler, R. G. Harley, "Power electronic converter and system control," *Proceedings of the IEEE*, vol.89, no.6, pp.913-925, Jun 2001
- [2] R. Lai, F. Wang, R. Burgos, Y. Pei, D. Boroyevich, B. Wang, T. A. Lipo, V. D. Immanuel, K. J. Karimi, "A Systematic Topology Evaluation Methodology for High-Density Three-Phase PWM AC-AC Converters," *IEEE Transactions on Power Electronics*, vol.23, no.6, pp.2665-2680, Nov. 2008
- [3] H. Mao, F. C. Lee, D. Boroyevich, S. Hiti, "Review of high-performance three-phase power-factor correction circuits," *IEEE Transactions on Industrial Electronics*, vol.44, no.4, pp.437-446, Aug 1997
- [4] M. Malinowski, M. P. Kazmierkowski, A. M. Trzynadlowski, "A comparative study of control techniques for PWM rectifiers in AC adjustable speed drives," *IEEE Transactions on Power Electronics*, vol.18, no.6, pp. 1390- 1396, Nov. 2003
- [5] S. Yang, Q. Lei, F. Z. Peng, Z. Qian, "A Robust Control Scheme for Grid-Connected Voltage-Source Inverters," *IEEE Transactions on Industrial Electronics*, vol.58, no.1, pp.202-212, Jan. 2011
- [6] Y. Sozer, D. A. Torrey, "Modeling and Control of Utility Interactive Inverters," *IEEE Transactions on Power Electronics*, vol.24, no.11, pp.2475-2483, Nov. 2009
- [7] Z. Chen, J. M. Guerrero, F. Blaabjerg, "A Review of the State of the Art of Power Electronics for Wind Turbines," *IEEE Transactions on Power Electronics*, vol.24, no.8, pp.1859-1875, Aug. 2009
- [8] L. Wu, Z. Zhao, J. Liu, "A Single-Stage Three-Phase Grid-Connected Photovoltaic System With Modified MPPT Method and Reactive Power Compensation," *IEEE Transactions on Energy Conversion*, vol.22, no.4, pp.881-886, Dec. 2007
- [9] V. Blasko, "Analysis of a hybrid PWM based on modified space-vector and triangle-comparison methods," *IEEE Transactions on Industrial Applications*, vol.33, no.3, pp.756-764, May/Jun 1997
- [10] K. Zhou, D. Wang, "Relationship between space-vector modulation and three-phase carrier-based PWM: a comprehensive analysis [three-phase inverters]," *IEEE Transactions on Industrial Electronics*, vol.49, no.1, pp.186-196, Feb 2002
- [11] A. M. Hava, R. J. Kerkman, T. A. Lipo, "Carrier-based PWM-VSI overmodulation strategies: analysis, comparison, and design," *IEEE Transactions on Power Electronics*, vol.13, no.4, pp.674-689, Jul 1998
- [12] A. M. Hava, R. J. Kerkman, T. A. Lipo, "Simple analytical and graphical methods for carrier-based PWM-VSI drives," *IEEE Transactions on Power Electronics*, vol.14, no.1, pp.49-61, Jan 1999
- [13] A. M. Trzynadlowski, R. L. Kirlin, S. F. Legowski, "Space vector PWM technique with minimum switching losses and a variable pulse rate [for VSI]," *IEEE Transactions on Industrial Electronics*, vol.44, no.2, pp.173-181, Apr 1997
- [14] R. L. Kirlin, C. Lascu, A. M. Trzynadlowski, "Shaping the Noise Spectrum in Power Electronic Converters," *IEEE Transactions on Industrial Electronics*, vol.58, no.7, pp.2780-2788, July 2011
- [15] L. Wei, et. "Pulse Width Modulation (PWM) Rectifier with Variable Switching Frequency", US patent 7190143132, Mar. 2007
- [16] D. Zhang, F. Wang, S. El-Barbari, J. Sabate, D. Boroyevich, "Improved asymmetric space vector modulation for voltage source converters with low carrier ratio," *Applied Power Electronics Conference and Exposition (APEC)*, 2010 Twenty-Fifth Annual IEEE, vol., no., pp.1487-1493, 21-25 Feb. 2010
- [17] R. Ghosh, G. Narayanan, "Control of Three-Phase, Four-Wire PWM Rectifier," *IEEE Transactions on Industrial Electronics*, vol.23, no.1, pp.96-106, Jan. 2008
- [18] D. Zhao, V. Hari, G. Narayanan, R. Ayyanar "Space-Vector-Based Hybrid Pulsewidth Modulation Techniques for Reduced Harmonic Distortion and Switching Loss," *IEEE Transactions on Power Electronics*, vol.20, no.3, pp.760-774, March 2010
- [19] D. Dujic, M. Jones, E. Levi, J. Prieto, F. Barrero, "Switching Ripple Characteristics of Space Vector PWM Schemes for Five-Phase Two-Level Voltage Source Inverters—Part 1: Flux Harmonic Distortion Factors," *IEEE Transactions on Industrial Electronics*, vol.58, no.7, pp.2789-2798, July 2011
- [20] M. Jones, D. Dujic, E. Levi, J. Prieto, F. Barrero, "Switching Ripple Characteristics of Space Vector PWM Schemes for Five-Phase Two-Level Voltage Source Inverters—Part 2: Current Ripple," *IEEE Transactions on Industrial Electronics*, vol.58, no.7, pp.2799-2808, July 2011
- [21] X. Mao, R. Ayyanar, H. k. Krishnamurthy, "Optimal Variable Switching Frequency Scheme for Reducing Switching Loss in Single-Phase Inverters Based on Time-Domain Ripple Analysis," *IEEE Transactions on Power Electronics*, vol.24, no.4, pp.991-1001, April 2009